RESEARCH   **Open Access**

Recombinant laccase rPOXA 1B real-time, accelerated and molecular dynamics stability study

Leidy D. Ardila-Leal[1], Pedro A. Monterey-Gutiérrez[2], Raúl A. Poutou-Piñales[1*] , Balkys E. Quevedo-Hidalgo[3*] , Johan F. Galindo[4*] and Aura M. Pedroza-Rodríguez[5]

Abstract

Background: Laccases (EC 1.10.3.2) are multi-copper oxidoreductases with great biotechnological importance due to their high oxidative potential and utility for removing synthetic dyes, oxidizing phenolic compounds, and degrading pesticides, among others.

Methods: A real-time stability study (RTS) was conducted for a year, by using enzyme concentrates from 3 batches (L1, L3, and L4). For which, five temperatures 243.15, 277.15, 298.15, 303.15, 308.15, and 313.15 K were assayed. Using RTS data and the Arrhenius equation, we calculated the rPOXA 1B accelerated stability (AS). Molecular dynamics (MD) computational study results were very close to those obtained experimentally at four different temperatures 241, 278, 298, and 314 K.

Results: In the RTS, 101.16, 115.81, 75.23, 46.09, 5.81, and 4.83% of the relative enzyme activity were recovered, at respective assayed temperatures. AS study, showed that rPOXA 1B is stable at 240.98 ± 5.38, 277.40 ± 1.32 or 297.53 ± 3.88 K; with $t_{1/2}$ values of 230.8, 46.2, and 12.6 months, respectively. Kinetic and thermodynamic parameters supported the high stability of rPOXA 1B, with an E_d value of 41.40 KJ mol^{-1}, a low variation of K_M and V_{max}, at 240.98 ± 5.38, and 297.53 ± 3.88 K, and ΔG values showing deactivation reaction does not occur. The MD indicates that fluctuations in loop, coils or loops with hydrophilic or intermediate polarity amino acids as well as in some residues of POXA 1B 3D structure, increases with temperature; changing from three fluctuating residues at 278 K to six residues at 298 K, and nine residues at 314 K.

Conclusions: Laccase rPOXA 1B demonstrated experimentally and computationally to be a stable enzyme, with $t_{1/2}$ of 230.8, 46.2 or 12.6 months, if it is preserved impure without preservatives at temperatures of 240.98 ± 5.38, 277.40 ± 1.32 or 297.53 ± 3.88 K respectively; this study could be of great utility for large scale producers.

Keywords: rPOXA 1B, Storage conditions, Laccase, Real-time stability, Accelerated stability, Molecular dynamics

* Correspondence: rpoutou@javeriana.edu.co; bquevedo@javeriana.edu.co; jfgalindoc@unal.edu.co
[1]Departamento de Microbiología. Facultad de Ciencias. Pontificia Universidad Javeriana (PUJ). Bogotá, Laboratorio de Biotecnología Molecular, Grupo de Biotecnología Ambiental e Industrial (GBAI), Bogotá, D.C, Colombia
[3]Departamento de Microbiología. Facultad de Ciencias. Pontificia Universidad Javeriana (PUJ), Laboratorio de Biotecnología Aplicada, Grupo de Biotecnología Ambiental e Industrial (GBAI), Bogotá, D.C, Colombia
[4]Departamento de Química, Universidad Nacional de Colombia, Bogotá, D.C, Colombia
Full list of author information is available at the end of the article

Background

Laccases (EC 1.10.3.2) are blue multi-copper oxidases (MCOs), usually monomeric and distributed in plants, insects, bacteria and fungi [1]. However, laccases from fungi have higher redox potentials (E_o) [2, 3], fostering oxidation of chemicals as mono, di-, poly- and methoxy phenols, aromatic and aliphatic amines, hydroxy indoles, benzenethiols and inorganic/organic metal compounds [4–6]. Due to laccases low specificity [7], they are attractive for different biotechnological applications, including juice clarification [8], biosensor manufacturing (for agri-environmental and biomedical applications) [9], sawdust biotransformation [10], coloured wastewater treatment [11–13], detoxification of cellulose pulp black liquor [14], simultaneous bioconversion of plastics and waste [15], biodeterioration of low-density plastics [16], and oxidation of micropollutants [17].

The laccases catalytic centre contains four copper atoms distributed over CuT1, CuT2 and CuT3 sites, located between cupredoxin-like domains 1 and 3 [1, 18]. Site CuT1 is mononuclear and coordinated with D3 residues. CuT1 is considered as the indicator of the redox potential of the enzyme [7, 19] because it captures electrons from the substrate and transferring them to the trinuclear copper centre (TNC) of the enzyme [20]. The TNC is composed of one copper from the CuT2 site (mononuclear) and two coppers from the CuT3 site (binuclear - CuT3α and CuT3β) [7]. Copper ions coordinate with the D1 and D3 domains located residues, where the reduction of O_2 to H_2O occurs [1, 19, 21].

Due to water production during catalysis, it has become a promising "green tool" for industrial and environmental applications. Therefore, its production and commercial availability must increase [3].

Knowing the thermal stability and storage conditions of any enzyme is of great importance to determine potential industrial applications [22, 23]. However, each enzyme has self-structure and stability, and it depends for the most part on its chemical environment as pH, ionic force, among others, temperature [24, 25]. Reasons for which, is remarkable to determine the most favourable storage conditions, as a function of the enzyme's shelf life [24], and to elucidate the necessity of incorporating preservatives agents to the final formulation.

For the study of the environment that favour enzyme and protein stability during storage, different conditions should be assayed (pH, temperature, NaCl concentration, presence of additives, preservatives and enzyme concentration, among others), [23]. Evaluating storage conditions at different temperatures is crucial since an increase in temperature augments the kinetic energy, leading to possible loss of enzyme activity and irreversible enzyme denaturation [26]. Additionally, it could also

result in dynamic changes in its 3D structure. These changes could be more or less aggressive, depending on the enzyme's thermostability [27].

Biological products are largely unstable; thus, it is customarily to store them under cold conditions. However, these storage conditions are not always the best as they involve high costs due to the maintenance of the cold chain [28]. Besides, enzyme denaturation can also occur under cold conditions [29]. Therefore, expiration dates are suggested based on collected real-time stability data. Accelerated stability studies are a complementary tool applied to proteins or enzymes with different applications [24].

Protein accelerated stability studies are performed usually at high temperatures (40 °C = 313.15 K), [24] as a tool to assess stability under adverse conditions [30]. Then employing Arrhenius formulas [31], the activation energy (E_a) and half-life ($t_{1/2}$) can be estimated; it is frequently for estimating protein and enzyme stability for pharmaceutical applications [24].

Accurate predictions of the thermal stability of enzymes and proteins are complex [32]. However, the combination of experimental results and computational analyses are effective for protein stability studies, as they allow rationalisation and interpretation of the experimental results [33]. Molecular dynamics (MD) simulations [34] explain the relationship between dynamics and the molecular mechanisms that stabilise the molecule under study through tools that measure flexibility and correlate it with function [33–35] as flexibility is a key property in protein activity and stability [36].

Some laccase MD analysis has focused on evaluating the influence of environmental conditions or the effect of the degree of glycosylation on structure, function and enzyme dynamics [18, 25]. Moreover, modified laccases by directed mutagenesis in the laboratory have been evaluating by MD [25, 37, 38].

The objectives of this work were, *i*) to propose the design of a more statistically based stability study, which would allow estimating at each sampling time with the same precision and confidence level the average enzyme activity (UL^{-1}) of rPOXA 1B laccase and thus support the stability study of other enzymes and proteins of non-pharmaceutical use [39], *ii*) use this statistical foundation to determine the real-time and accelerated stability of the recombinant rPOXA 1B enzyme from *P. ostreatus* produced in *P. pastoris* and *iii*) relate the real-time-stability with the in silico behaviour of the enzyme during molecular dynamics simulations.

Materials and methods

Pilot study of enzyme stability

To estimate rPOXA1B enzyme activity (UL^{-1}) variability at different temperatures a pilot study was performed.

Fifteen vials were prepared (2 mL polypropylene screw-cap Microtube BIOLOGIX) containing 1 mL rPOXA 1B concentrate with an enzyme activity of 5877.31 ± 278.11 UL^{-1} (∼ 164.62 Umg^{-1}) placed at – 30, 4, 30, 40 and 50 °C, equivalent to absolute theoretical temperatures of 243.15, 277.15, 303.15, 313.15 and 323.15 K, respectively. Temperatures were selected based on a previous thermal stability study performed for 1 h of enzyme exposure [40]. Enzyme activity (UL^{-1}), [41], was measured at days 0, 15 and 30 (each one considered a sampling time), for each temperature. Sampling was performed at random, using a generator of random numbers with Stata V.14. Pilot study results were used to define the vial population size (*N*) and from this one, for each sampling time a sample size (*n*) was calculated. Estimated variances in the pilot study were used to appraise the variability of the process. Moreover, assuming homogeneity of variance, its combined variance was calculated with a similar statistical analysis as is used to estimate variance for a *t*-test for equal variances.

rPOXA 1B concentrate batches

We use *P. pastoris X33/pGAPZαA-LaccPost-Stop Clone 1* [42] to produce rPOXA 1B batches on a 10 L bioreactor scale; following the production and concentration methodology previously described [40]. For the study, we used three random selected batches (L1, L3 and L4), wich enzyme activity per concentrate batch (preservative-free), were L1: 27,222.2 UL^{-1}; L3: 37,222.2 UL^{-1} and L4: 34,236.1 UL^{-1}. Every batch was diluted with distilled water to match the initial enzyme activity of 16,575.50 ± 268.92 UL^{-1} (758.71 ± 180.18 Umg^{-1}), time zero of the study without sampling.

rPOXA 1B stability study: design and conditions

Based on the pilot stability study results, five temperatures were selected [243.15 K (stored in the freezer), 277.15 K (stored in the refrigerator), 298.15, 303.15, 308.15 and 313.15 K (stored in independent incubators)]. A thermo-hygrometer placed in each incubation equipment allows daily monitoring of temperature and relative humidity (RH) expressed in %, except for – 30 °C (243.15 K) and 4 °C (277.15 K) at which humidity is normally high. Temperature and RH values obtained throughout the study (1 year) were transformed to K and averaged at the end of the stability study to calculate both standard deviation (SD) during the length of the stability study. The stability study has a monthly periodicity (30 calendar days) until the first 6 months and later, every 2 months (60 days) to complete a year. However, the number of samples by temperatures varied according to enzyme activity loss. A relative enzyme activity loss of about ∼ 75% was set up as the limit for sampling. Nonetheless, when enzyme activity loss exceeded before the

end of the sampling time assigned; a minimum of five sampling times was established (whenever possible).

A stratified sampling strategy allows estimating the enzyme activity (UL^{-1}) average at different sampling moments for each temperature. The initial population (time 0) at each temperature, consisted of three batches (L1, L3 and L4) with the same number of vials, containing 2 mL polypropylene screw cap tube (BIOLOGIX) with one millilitre of recombinant enzyme concentrate from each respective batch (L1, L3, L4). Vials of each batch were stored in two square cryopreservation boxes (10 × 10 vials). Each batch constructed constituted a selection stratum for each sampling time.

An Excel spreadsheet was programmed to determine population size (N), varied population sizes were assigned and tested to estimate the mean value in the stratified sampling with proportional allocation, using different levels of precision and confidence, and considering the costs that designs would entail [43]. Finally, the population size calculated was assumed for the three strata (L1, L3 and L4), allowing to estimate the median value of the enzymatic activity of rPOXA1B (UL^{-1}) for each sampling moment, with a precision of 21.8 (UL^{-1}) and 95% confidence.

According to stratified sampling, a simple random sample was taken from each batch at each sampling time, to estimate the average enzyme activity of rPOXA 1B (UL^{-1}) and its corresponding confidence interval (CI). For estimations, we used stratified probability sampling bases with proportional allocation [43].

Sampled vials at each time of the stability study allow to determining enzyme activity (UL^{-1}). Later, the rest of the sample of the same time point and temperature were pool to determine by triplicate apparent V_{max} and K_M, with their respective ANOVA analysis using SPSS 19. To determining V_{max} and significant differences, a 0.05 significance was established for the temperature range assayed.

Real-time stability of rPOXA 1B

Real-time stability of rPOXA 1B, was determined by plotting (isotherms) average enzyme activities ± confidence interval (CI) for each sample, at each sampling time. To this object SigmaPlot V11.0., was used. Relative enzyme activity was the percentage of activity recovered at each sampling time, compared to the initial volumetric enzyme activity (100%).

rPOXA 1B accelerated stability analysis and thermodynamic parameters

The slope from the Ln (E/E_o) graph as a function of time (months), based on the enzyme activity (UL^{-1}) analysis of the first-order kinetics for each of the isotherms (243.15, 277.15, 298.15, 303.15, 308.15 and 313.15 K)

Ardila-Leal *et al. BMC Biotechnology*   (2021) 21:37

Page 4 of 18

allows calculating the inactivation rate constant (k_d). E_0 is the initial enzyme activity (UL^{-1}) and (E) is the average enzyme activity (UL^{-1}) for each sampling time. Deactivation energy (E_d) was calculated by plotting the Ln (k_d) graph obtained for each isotherm versus the inverse of the temperature (1/T) in K, using Arrhenius (Eq. 1).

The enzyme's half-life ($t_{1/2}$) is the time required for the enzyme to decrease in half its initial activity [31], and by using (Eq. 2) it was calculated.

Thermodynamic parameters ΔH (change in enthalpy of deactivation), (Eq. 3), ΔG (change in Gibb's free energy of inactivation), (Eq. 4) and ΔS (change in entropy of inactivation), (Eq. 5) for an irreversible inactivation were calculated from the following equations.

$$\ln (k_d) = \ln (A) - \frac{E_d}{RT} \tag{1}$$

$$t_{1/2} = \frac{\ln 2}{k_d} \tag{2}$$

$$\Delta H = E_d - RT \tag{3}$$

$$\Delta G = -RT \ln \left(\frac{k_d h}{k_b T} \right) \tag{4}$$

$$\Delta S = \frac{(\Delta H - \Delta G)}{T} \tag{5}$$

Where: k_d is the deactivation constant, A is the frequency factor, E_d is the deactivation energy, R is the universal gas constant ($8.314\,J\,mol^{-1}\,K^{-1}$), and T is the absolute temperature (Kelvin) [31, 44], h is the constant of Plank ($6.626 \times 10^{-34}\,J\,s$) and k_b is the constant Boltzmann ($1.38 \times 10^{-23}\,JK^{-1}$), [44, 45].

Determination of laccase activity

Laccase enzyme activity was determined using ABTS (2,-Azino-bis(3-ethylbenzothiazoline-6 sulfonic acid) as a substrate. Into a 100 μL spectrophotometric cuvette 20 mM ABTS and centrifuged supernatant (from 2 to 20 μL, depending on the amount of enzyme present in the sample were added). To complete a final volume of 1 mL 0.1 M citrate buffer (pH 3.0 ± 0.2) was added. One-minute absorbance change resulting from ABTS oxidation at 420 nm was measured [41]. One unit of the enzyme (U) is defined as the quantity of enzyme capable of transforming 1 μmol ABTS substrate per minute, per litre, and was calculated based on (Eq. 6).

$$UL^{-1} = \frac{(\Delta E \times V_t)}{(\varepsilon \times d \times V_s)} \tag{6}$$

Where: ΔE corresponds to the difference between final and initial absorbance after 1 min of reaction, V_t refers to the total reaction volume (mL), ε refers to the ABTS molar extinction coefficient ($M^{-1}\,cm^{-1}$) at 420 nm, d is the length of the cuvette in cm and V_s is the volume of sample (mL) contained in the reaction.

Apparent enzyme kinetic constants

As the real-time stability study progressed and once laccase activity was quantified, at each sampling moment, the remaining volume of samples (n) were pool (distinguishing by batch, by temperature, by sampling time) to determine the kinetics of the enzyme. For the enzyme kinetic assay ABTS dissolved in 0.1 M citrate buffer, was used as a substrate (concentration between 0.1–3 mM), pH 3.0 ± 0.2. An enzyme solution with an activity of 10 UL^{-1} at 25 °C [46]. All kinetic tests performed in triplicate. The experimental data from each enzyme kinetic were feed to Biomodel software (http://biomodel.uah.es/metab/enzimas/inicio.htm), which allows fitting the experimental data to the Michaelis-Menten equation (Eq. 7) using a non-linear, least-squares based regression. K_M and V_{max} values previously estimated by the Hanes-Woolf linear regression (Eq. 8), [47] by using SIMFIT software (V7.6.8), [48] used to start the iteration process at Biomodel.

$$V_0 = \frac{V_{max}[S]}{K_M + [S]} \tag{7}$$

$$\frac{[S]}{V_0} = \frac{[S]}{V_{max}} + \frac{K_M}{V_{max}} \tag{8}$$

Where: V_0 is the initial velocity, V_{max} is the maximum reaction rate, K_M is the Michaelis constant and [S] is the substrate concentration.

Homology modeling of POXA 1B

Since there is no crystal structure reported for POXA1B from *Pleurotus ostreatus* it was necessary to create a 3D model for the enzyme; then the sequence was processed in the SignalP 5.0 server (http://www.cbs.dtu.dk/services/SignalP/) to identify and eliminate peptide signal amino acids.

Laccase 3D structure was predicted by homology modelling [42, 49–51] using the HHpred, Phyre2 and Swiss-model servers. The resulting model was evaluated by QMEAN [52, 53] and for characteristics of the enzyme's

active site. Saves V 5.0 server allows validating the quality of the modelled structure (https://servicesn.mbi.ucla.edu/SAVES/).

POXA 1B molecular dynamics simulations at different temperatures

The CuT1 copper and TNC in laccase's binding pocket were parametrized, by using the metal centre parameter builder (MCPB.py), [54] included in the Amber18 package [55], the partial charges were obtained from the electrostatic calculation by using Gaussian 16 [56]. A complete set of the parameters generated by mcpb.py for cooper ions and their coordination residues are in Supplementary Material S1. All coppers (Cu type I and Cu from TNC) were modelled as Cu^{2+}. The hydrogens and protonation state for each residue were carried out with webserver H++ (http://biophysics.cs.vt.edu/) adjusting the PDB file of POXA 1B to pH 3.0. For MD simulations topology files and system, coordinates were prepared using the tleap interface. The system was neutralized with Na^+ and Cl^- and was immersed in a TIP3P water box with 10.0 Å between any atom of the protein and the edge of the box. Additionally, the ff14SB force field was used to model all amino acid residues [57].

To compare the stability of the enzyme at different temperatures, four temperatures were set up [241 K (−32 °C); 278 K (5 °C); 298 K (25 °C) and 314 K (41 °C)]. Initial energy minimization was carried out, using 50,000 steps of the steepest descent algorithm steps, followed by 10,000 steps of conjugate gradients. The minimized system was gradually warmed up to four stages from 0 to 241 K (stage 1), from 241 to 278 K (stage 2), from 278 to 298 K (stage 3) and from 298 to 314 K (stage 4); using an NVT canonical ensemble and a Langevin thermostat with a 2.0 ps^{-1} collision frequency and a 2 fs step size Newton equations were integrated.

All simulations were performed with the same cut-off and electrostatic interactions beyond the cut-off distance are ignored. In all simulations, a cut-off of 8.0 Å was employed for both the electrostatics and the van der Waals interactions. The imposition of periodic boundaries on the system during the calculation was controlled at constant pressure with isotropic position scaling and in the production were kept the coordinate output from overflowing the trajectory.

With the results obtained from each of the heating stages, were evaluated several MD stages. The density of each heating step was equilibrated for 400 and 200 ns production and simulated using an isothermal-isobaric (NPT), hydrogen length constrained (SHAKE) assembly. Snapshots of the scenario were taken every 0.2 ns during production (1000 in total). The trajectories obtained for each temperature were analysed using CPPTRAJ [58, 59].

Principal component analysis

To evaluate movements of the main chains of the system for the four temperatures studied principal component analysis (PCA) was carried out, according to previously described methodology [60]. The covariance matrix was constructed from MD topology and trajectory obtained files. The root mean square (RMS) was adjusted to eliminate rotational/translational movements and preserve internal dynamics, except for hydrogen atoms. The first five principal components corresponding to the first eigenvectors of the covariance matrix were selected. Structural representations of the different modes were constructed in CPPTRAJ and visualized in Visual Molecular Dynamics (VMD). Additionally, for the PCA a superposition of Cα atoms in the MD trajectories using R's Bio3D package [61] was constructed from which the contribution of each residue was evaluated for the first five main PCAs [59].

Results

Pilot study of enzyme stability

The stability pilot assay demonstrated that as the temperature increased, the relative activity of the enzyme decreased. Between 243.15 K (− 30 °C) and 277.15 K (4 °C) there were slight enzyme activity variations at day 30 of the study. At 303.15 K (30 °C) relative enzyme activity was maintained (∼ 85%); whereas at 313.15 K (40 °C) and 323.15 K (50 °C), temperatures were destabilizing for the system, with a considerable reduction of the enzyme activity (Table 1).

Assuming equal variances for each temperature, a combined variance estimator (an estimator commonly used in parametric tests) was used to obtain an estimate of enzyme activity variability; with an estimate of 96.6 for rPOXA 1B UL^{-1} standard deviation.

Real-time stability of rPOXA 1B concentrate

Table 2 illustrates population size (N) and sample size (n), at the beginning of the study (month 0) and at each sampling time (months). For the theoretical temperatures of 30 and 4 °C averages of 240.98 ± 5.38 K (− 32.55 ± 4.12 °C) and 277.40 ± 1.32 K (4.32 ± 1.22 °C) were

Table 1 Percentage of rPOXA 1B relative activity preserved during 30 days at five theoretical study temperatures

Temperature °C	Temperature K	Time (days)	
		15	30
		% relative enzyme activity	
−30	243.15	95.38	96.74
4	277.15	88.50	95.36
30	303.15	84.76	85.59
40	313.15	74.05	61.30
50	323.15	25.96	13.39

Table 2 Sampling distribution carried out for each lot and sampling time

Month	Sampling time	N	n
1	1	200	16
2	2	184	16
3	3	168	16
4	4	152	16
5	5	136	16
6	6	120	15
8	7	105	15
10	8	90	15
12	9	75	14

N: Population size, *n*: sampling size

obtained, and the 12 months of the study were completed. For the theoretical temperatures of 25, 30, 35 and 40 °C, averages of 297.53 ± 3.88 K (24.99 ± 0.25 °C), 303.27 ± 1.11 K (30.12 ± 1.11 °C), 309.58 ± 0.23 K (36.43 ± 0.23 °C) and 314.79 ± 0.52 K (41.64 ± 0.52 °C) were obtained.

Figure 1, depicts relative enzyme activity ± confidence interval and in Table 3 rPOXA 1B specific activity (U mg^{-1}) ± confidence interval (CI), as a function of time exposed to different study temperatures. At 240.98 ± 5.38 K, it was observed the activity remained constant

throughout the 12 months of the study. At 277.40 ± 1.32 K, a slight increase in enzyme activity percentage was observed after the sixth month of sampling. For the temperatures of 297.53 ± 3.88, 303.27 ± 1.11 and 309.58 ± 0.23 K, a slight gradual reduction in enzyme activity was observed as the temperature increased, maintaining a residual enzyme activity of 75.23, 46.09 and 5.81%, respectively, until the last sample. At 314.79 ± 0.52 K, a considerable loss in relative enzyme activity was observed for the first month of sampling, with a residual enzyme activity of 4.83% (Fig. 1, Table 3).

rPOXA 1B accelerated stability and thermodynamics parameter analysis

Accelerated stability calculations were obtained as a function of time, and rPOXA1B deactivation using different exposure temperatures. First-order deactivation kinetic yielded the enzymatic deactivation constant (k_d), (Fig. 2, Table 4) with R^2 between 0.9710 and 0.8810. Half-life ($t_{1/2}$) and deactivation energy (E_d) (Fig. 3, Table 4) were calculated from obtained k_d at different temperatures.

The thermodynamic parameters to identify the stability of rPOXA 1B appears in Table 4. ΔH was constant over the study range, as the ΔH values only decreased by approximately 1.5% with increasing temperature by 70 K; this variation is within the experimental uncertainty.
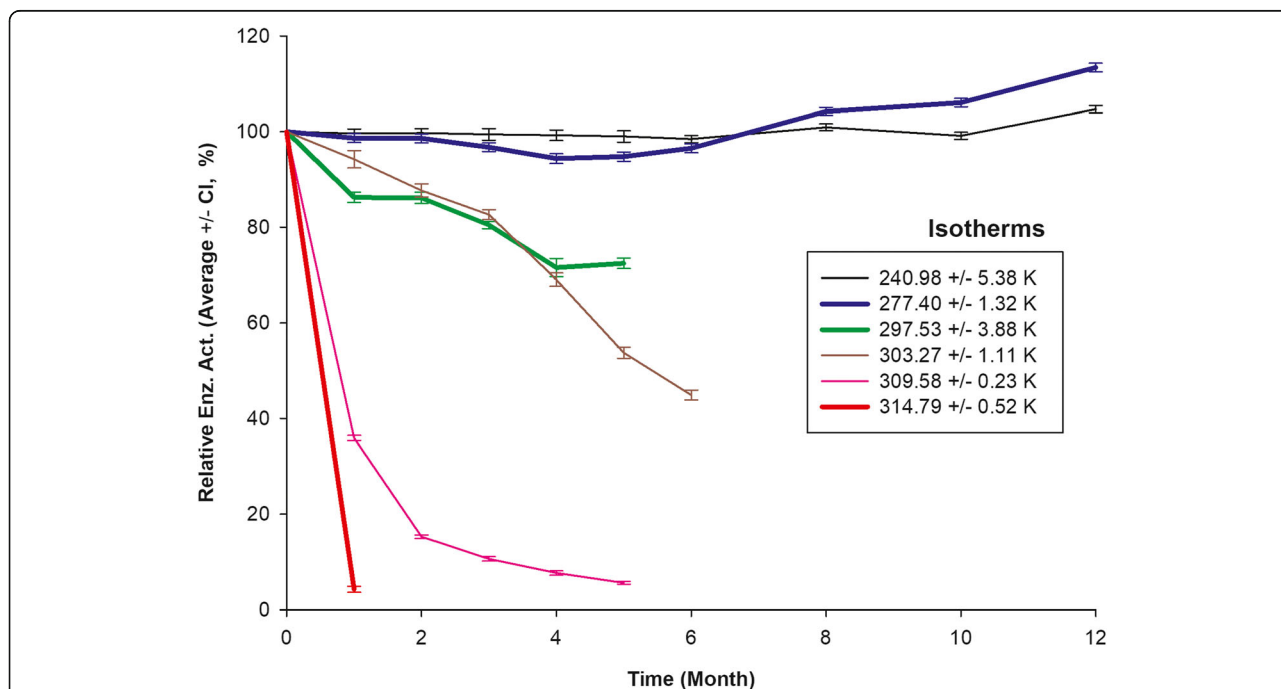

Fig. 1 rPOXA 1B real-time enzyme stability study. Percentage of relative enzyme activity isotherms of the L1, L3 and L4 batches average ± CI of vs., time in months for each assayed temperature. The three temperatures with the thickest lines (blue, green and red) are those studied computationally. The enzyme activity (UL^{-1}) was averaged, at each sample, batch and storage temperatures. The average enzyme activity allows estimating the percentage of relative enzyme activity concerning the initial enzyme activity

Table 3 Specific activity (U mg^{-1} ± CI) during sampling months

Temperature K	240.98 ± 5.38	277.40 ± 1.32	297.53 ± 3.88	303.27 ± 1.11	309.58 ± 0.23
Temperature °C	−32.55 ± 4.12	4.32 ± 1.22	24.99 ± 0.25	30.12 ± 1.11	36.43 ± 0.23
Time (Month)	Specific Activity U mg^{-1} ± CI				
1	758.92 ± 8.90	857.23 ± 10.09	745.57 ± 12.32	759.46 ± 16.71	236.74 ± 4.07
2	763.62 ± 7.75	872.88 ± 9.77	737.70 ± 12.11	679.41 ± 11.49	116.74 ± 2.71
3	752.30 ± 9.54	863.89 ± 9.64	663.10 ± 11.70	627.46 ± 10.27	76.87 ± 3.09
4	758.06 ± 9.03	860.29 ± 10.13	587.68 ± 14.01	520.02 ± 10.29	54.15 ± 2.86
5	754.66 ± 9.95	878.27 ± 9.78	567.65 ± 13.30	395.92 ± 9.83	37.65 ± 1.99
6	763.25 ± 6.38	884.82 ± 10.15	563.05 ± 0.0		
8	787.08 ± 6.27	959.30 ± 10.84			
10	759.43 ± 6.30	997.01 ± 13.22			
12	934.81 ± 9.70	1045.58 ± 15.31			

The ΔG showed high and positive values, while ΔS exhibited negative values.

Effect of different temperatures on (apparent) V_{max} and K_M

Observed apparent V_{max} and K_M appear in Table 5. V_{max} for enzymes at different temperatures revealed that between 240.98 ± 5.38 and 297.53 ± 3.88 K no variation was observed, whereas it decreased for higher temperatures (309.58 ± 0.23 and 314.79 ± 0.52 K). K_M variation was associated with exposure temperature, increasing as exposure temperature augmented. For both analyses, differences between temperatures were significant (Table 5).

Homology model of POXA 1B

Evaluated servers generated different predictions for POXA1B 3D's protein structure from amino acid sequences. However, among servers, the predictions obtained from HHpred and Phyre2 did not result in a model according to the distribution of copper atoms at the site of the enzyme. Therefore, we decided to evaluate different predicted models using an automated comparative 3D protein modelling server SWISS-MODEL [62, 63]. The SWISS-MODEL template library was searched with BLAST [64] and HHBlits [65].

Templates for POXA 1B modelling and models obtained from 5Z1X (*Cerrena* sp. RSD1), 5E9N (*Steccherinum murashkinskyi*) and 1GYC (*Trametes versicolor*) were evaluated, with identities of 64.12, 62.96 and 62.50%, respectively. The characteristics of the active were evaluated and it was observed the 1GYC template had a more suitable configuration at the active site. The model obtained with the selected template obtain a 0.80 QMEAM and a GMQE of 0.87. Predicted results for the model are in Supplementary Material Figure 1. Validation of the structure was supported by Saves 5.0 model structure scores, which according to Ramachandran's plot revealed t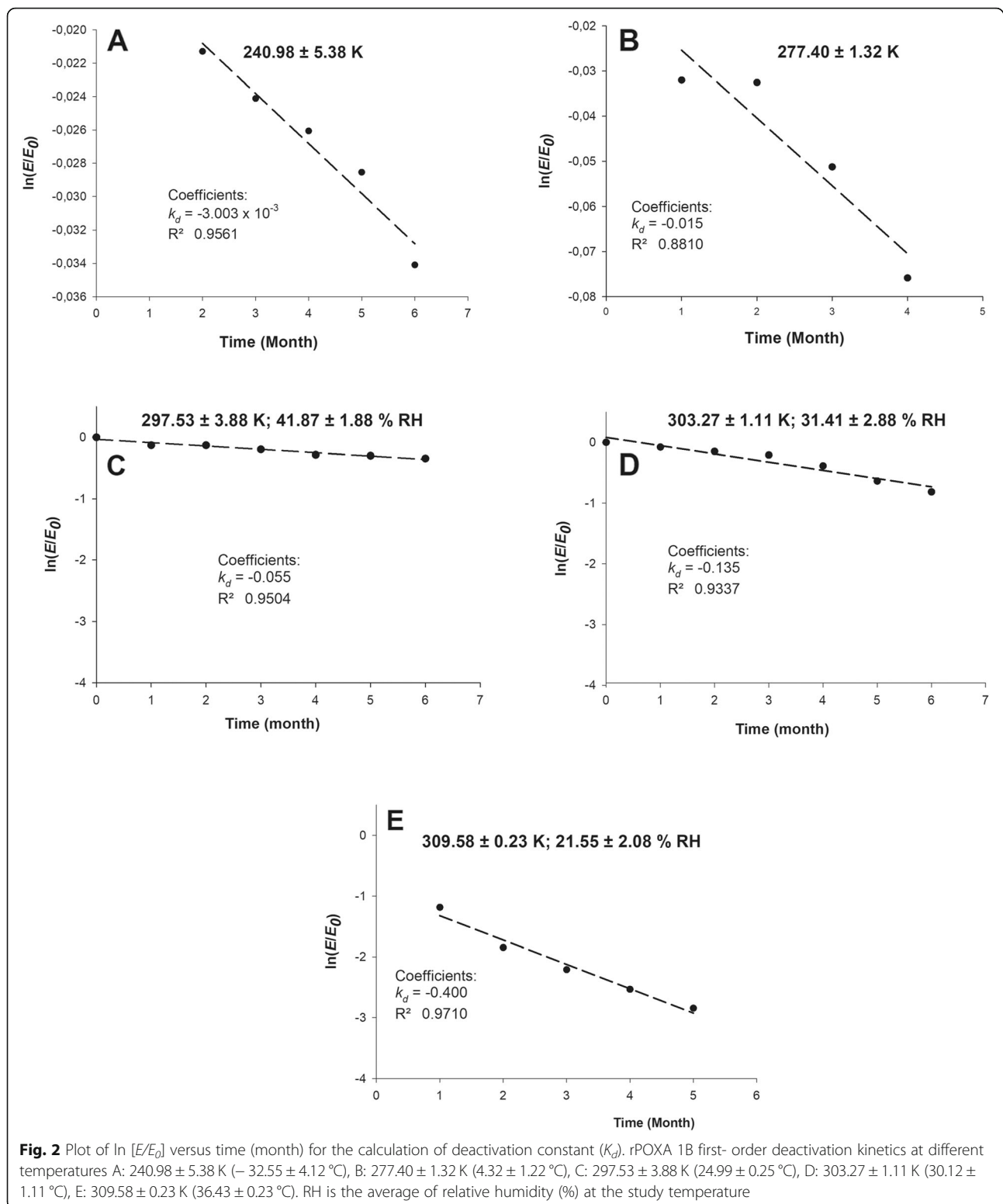hat 88.9% of the residues were in the most favoured region and 10.6% in the additional allowed region (Supplementary Material Figure 2). Verify 3D score was 94.08%, ERRAT score was 88.7734 and the PROVES score was 4.1%.

Molecular dynamics simulations and PCA analysis

In the active site parametrization, CuT1 copper was coordinated with His^{394}, HIS^{496} and CYS^{451}. Distance between CuT1 and the TNC was approximately 12 Å. CuT2 was coordinated with HIS^{64}, HIS^{397} and a hydroxyl group. CuT3 coppers were coordinated with six histidines (HIS^{66}, HIS^{109}, HIS^{111}, HIS^{399}, HIS^{450}, HIS^{452}) and a hydroxyl group between CuT3 and CuT3 (Supplementary Material Figure 3).

To evaluate the effect temperature (241 K [− 32 °C], 278 K [5 °C], 298 [25 °C] K and 314 K [41 °C]) had on the enzyme, MD simulations were performed. Simulated system stability at different temperatures was evaluated by calculating the root-mean-square deviation (RMSD) during the simulation time. It was observed that the conformational stability of the systems was maintained during the simulations since the deviation did not exceed 2 Å for all evaluated temperatures (Supplementary Material Figure 4). Furthermore, it was noticed deviations increased as the simulation temperature was raised. Thus, the higher deviations corresponded to 314 K (40.85 °C), (Supplementary Material Figure 4).

The structural changes responsible for the system's destabilization were determined by calculating the average root mean square fluctuations (RMSF) for each of the simulated temperatures. During the MD simulation, each residue's fluctuation (RMSF) was analyzed (Supplementary Material Figure 5). In addition, a comparison by residue between the different temperatures an Δ RMSF was calculated considering as reference the lowest temperature (278–241 K, 298–241 K and 314–241 K), Fig. 4A. The aforementioned facilitated identifying the regions and/or residues leading to fluctuations as a

Fig. 2 Plot of ln [E/E_0] versus time (month) for the calculation of deactivation constant (K_d). rPOXA 1B first- order deactivation kinetics at different temperatures A: 240.98 ± 5.38 K (− 32.55 ± 4.12 °C), B: 277.40 ± 1.32 K (4.32 ± 1.22 °C), C: 297.53 ± 3.88 K (24.99 ± 0.25 °C), D: 303.27 ± 1.11 K (30.12 ± 1.11 °C), E: 309.58 ± 0.23 K (36.43 ± 0.23 °C). RH is the average of relative humidity (%) at the study temperature

function of temperature in the simulation. In Fig. 4A two negative peaks were observed for Δ RMSF at 278, 298 and 314 K corresponding to LYS[309] and ALA[363] amino acids (Violet beads - Fig. 5), which indicate the

fluctuation was less in comparison with the temperature at 241 K. Moreover, Δ RMSF 298 K an additional negative peak corresponding to residue SER[412] was observed. On the other hand, it was recognized the number of

Table 4 rPOXA 1B concentrate (enzyme without purification) thermodynamic parameters, calculated during thermal deactivation at study temperatures.

Thermodynamic parameters	Temperature K				
	240.98 ± 5.38	277.40 ± 1.32	297.53 ± 3.88	303.27 ± 1.11	309.58 ± 0.23
	Temperature °C				
	−32.55 ± 4.12	4.32 ± 1.22	24.99 ± 0.25	30.12 ± 1.11	36.43 ± 0.23
K_d (months^{-1})	3×10^{-3}	0.015	0.055	0.135	0.400
$t_{1/2}$ (months)	230.8	46.2	12.6	5.1	1.7
E_d (kJ mol^{-1})	41.40				
ΔH (kJ mol^{-1})	39.40	39.10	38.93	38.88	38.83
ΔG (kJ mol^{-1})	70.23	77.46	80.04	79.37	78.28
ΔS (J mol^{-1} K^{-1})	−127.94	− 138.30	−138.17	− 133.50	− 127.42

residues with the biggest fluctuations augmented with increasing temperature.

For Δ RMSF 278 K, in Figs. 4A and 5A, it was observed residues LEU[159], ALA[391] and ASP[429] (Orange beads – Fig. 5A) presented the highest fluctuations, and the residues in proximity to LEU[159] and ASP[429] generated fluctuating regions. Figures 4A and 5B for Δ RMSF 298 K residues with high fluctuations were THR[160], ASP[266], GLU[293], ALA[334], ASP[341] and LEU[459] (Orange beads – Fig. 5B), only amino acids close to ALA[334] conformed a fluctuating region (Yellow region - Fig. 5B). In Figs. 4A and 5C, for Δ RMSF 314 K residues with high fluctuation increased, where ASP[101], THR[160], GLY[265], ASN[297], ALA[334], GLY[370], ALA[391], PRO[393] and ASP[433] were of the greatest fluctuation (Orange beads – Fig. 5).

Likewise, residues close to THR[160], ASN[297], ALA[334] and ASP[433] generated fluctuating regions (Yellow region - Fig. 5C).

Residues and regions with Δ RMSF that increased fluctuation in a progressive manner, according to the increase in temperature, were identified as ASP[266], with its region in the vicinity between SER[264] - PHE[269]; and ASN[297] with its region in the vicinity between GLN[293] - PRO[298]. Standard deviation calculation among Δ RMSF revealed the residues with standard deviations greater than 0.5 Å (cut off point) corresponded to the same previously identified residues, including the additional residues ALA[391] and PRO[393].

RMSF and PCA supported residue contribution to the system's atomic fluctuation variations. The PCA was

Coefficients:
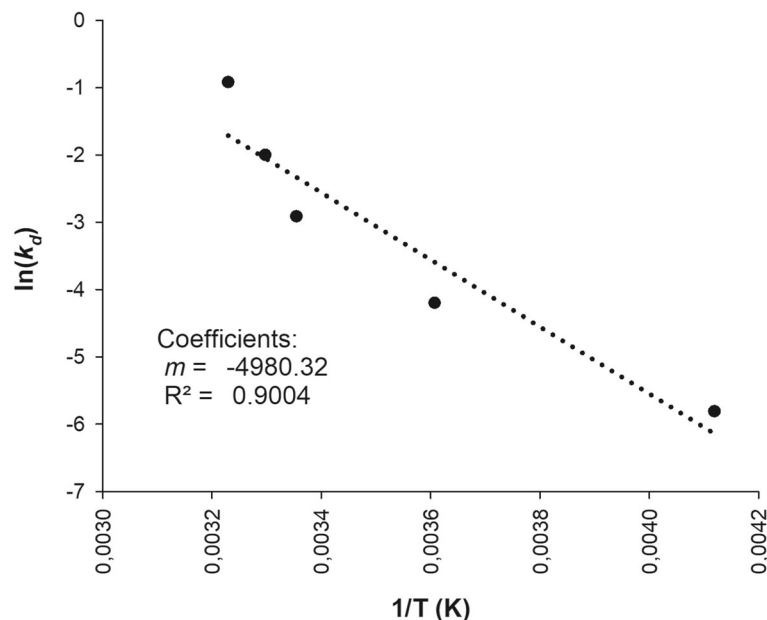m = −4980.32
R² = 0.9004

Fig. 3 Arrhenius plot to get deactivation energy (E_d) calculation of rPOXA 1B exposition temperatures between 240.98 ± 5.38 K (− 32.55 ± 4.12 °C) and 309.58 ± 0.23 K (36.43 ± 0.23 °C)

Table 5 Apparent V_{max} and K_M average variation after X time exposure at different temperatures

Temperature[a]		Time	Number of	Non-linear, least-squares based regression	
				$V_{max} \pm SD$	$K_M \pm SD$
(°C)	(K)	(Month)	(pool)	(mM min^{-1})	(mM)
−32.55 ± 4.12	240.98 ± 5.38	12	27	0.0102 ± 0.0004	0.0414 ± 0.0046
4.32 ± 1.22	277.40 ± 1.32	12	27	0.0104 ± 0.0005	0.0435 ± 0.0057
24.99 ± 0.25	297.53 ± 3.88	6	18	0.0102 ± 0.0004	0.0466 ± 0.0064
30.12 ± 1.11	303.27 ± 1.11	6	18	0.0104 ± 0.0004	0.0477 ± 0.0076
36.43 ± 0.23	309.58 ± 0.23	4	12	0.0094 ± 0.0005	0.1016 ± 0.0736
41.64 ± 0.52	314.79 ± 0.52	1	3	0.0096 ± 0.0006	0.1433 ± 0.1564

[a]Temperatures at which the samples were stored during the real-time stability study

Kinetic enzymatic reaction conditions were ABTS dissolved in 0.1 M citrate buffer at concentration between 0.1–3 mM, pH 3.0 ± 0.2. An enzyme solution with an activity of 10 UL^{-1}, reaction temperature 25 °C
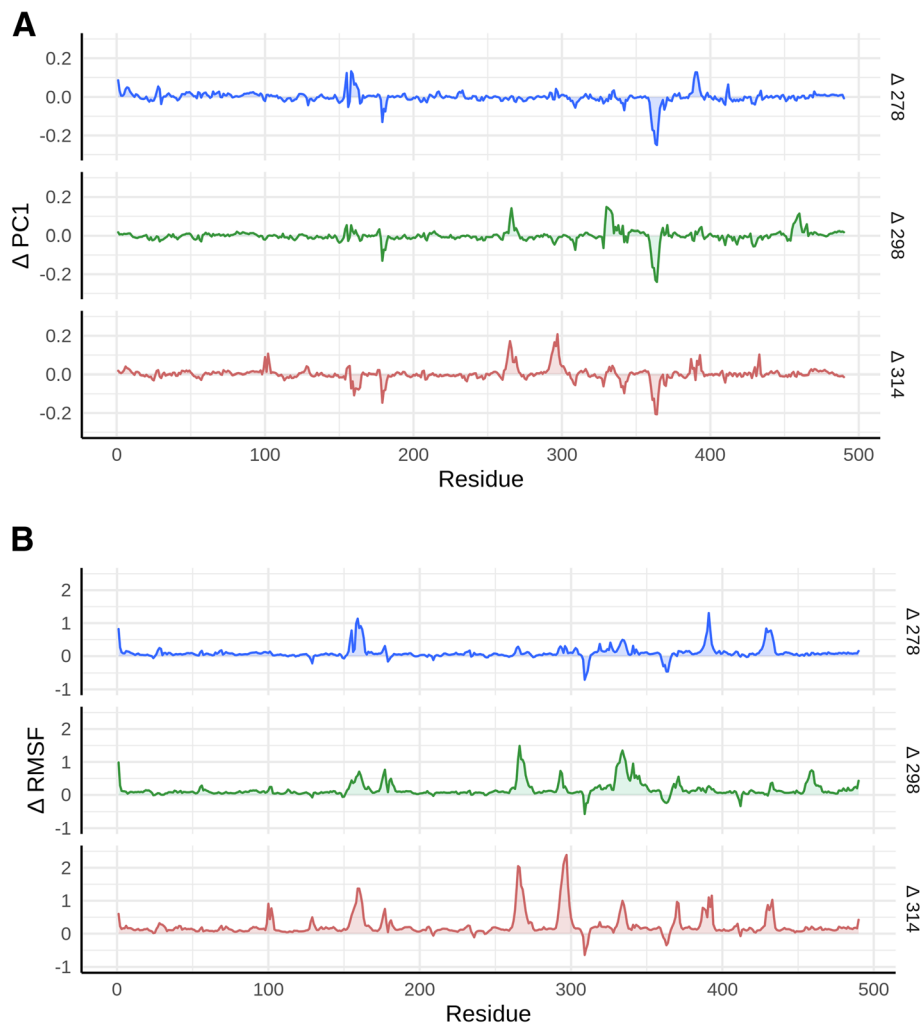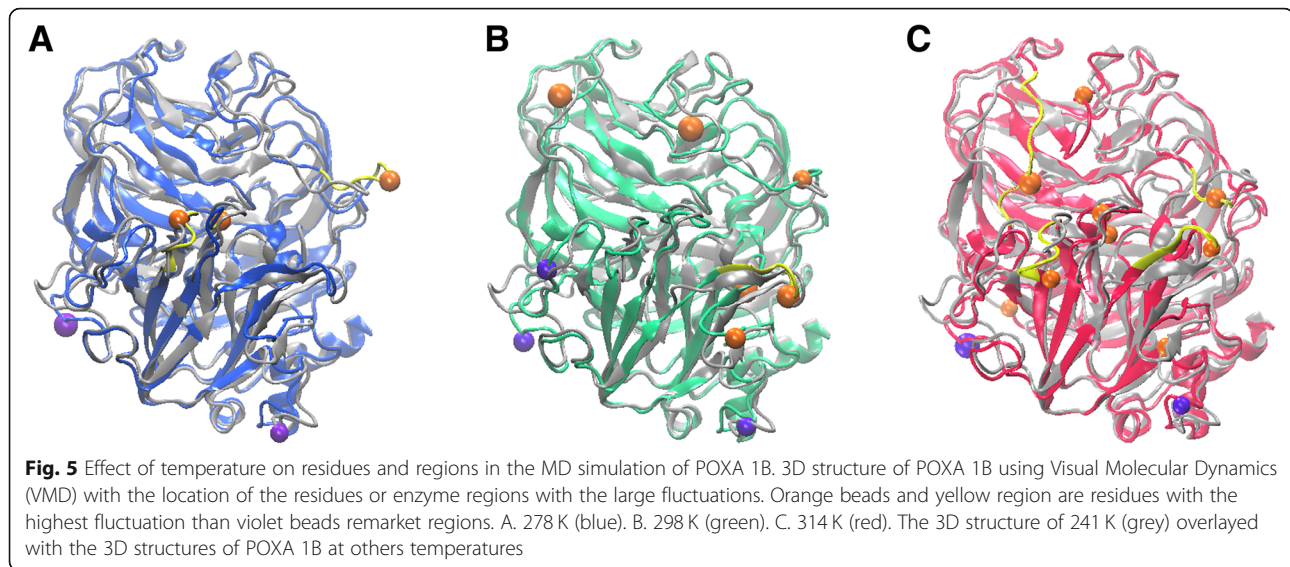

Fig. 4 Comparison of the RMSF differences (Δ RMSF) calculated between the different study temperatures against 241 K. In the Δ RMSFs, a positive value indicates that the residual has fluctuations, and a negative value indicates the opposite A. Δ RMSF (278–241 K blue; 278–241 K green and 314–241 K red). B. Δ PC1 (278–241 K blue; 278–241 K green and 314–241 K red). The protein skeleton (C, CA and N), averaged per residue, was used to calculate the RMSF

Fig. 5 Effect of temperature on residues and regions in the MD simulation of POXA 1B. 3D structure of POXA 1B using Visual Molecular Dynamics (VMD) with the location of the residues or enzyme regions with the large fluctuations. Orange beads and yellow region are residues with the highest fluctuation than violet beads remarket regions. A. 278 K (blue). B. 298 K (green). C. 314 K (red). The 3D structure of 241 K (grey) overlayed with the 3D structures of POXA 1B at others temperatures

performed using C position co-variance to describe the global movements of rPOXA 1B at different temperatures employing the first principal components (PC).

Furthermore, to make a comparison by residue the first Δ PC was calculated considering as reference the lowest temperature; for instance, 278–241 K, 298–241 K and 314–241 K. In Fig. 4B, Δ PC1 are depicted for 278–241 K, 298–241 K and 314–241 K, which included previously observed residues and regions in the Δ RMSF. For Δ PC1 278 K the included residue was ALA^{391} and the included regions were PRO^{155} - THR^{160} and THR^{360} - ASP^{365}. For Δ PC1 298 K the residue was ASP^{266} and the regions ALA^{330} - ALA^{334}, THR^{360} - ASP^{365} and ASP^{458} - GLY^{460}. For Δ PC1 314 the residues were GLU^{101}, THR^{160}, PRO^{393}, ASP^{433} and the regions ASN^{263} - PRO^{267}, GLN^{293} - PRO^{298}, THR^{360} - ASP^{365}. PC1 represented 15.4, 15.9, 11.8 and 18.6% variance proportion for 241 K (– 32 °C), 278 K (5 °C), 298 K (25 °C) and 314 K (41 °C), respectively.

Δ PC2 and Δ PC3 were calculated similarly to Δ PC1 (Supplementary Material Figure 7) and included the missing residues that showed fluctuation in the Δ RMSF and were not represented in Δ PC1. The first five components accounted for approximately 41% of the variations at 241 K (– 32.15 °C), 278 K (4.85 °C) and 314 K (40.85 °C) and ~ 36% of the variations at 298 K (24.85 °C) (Supplementary Material Figure 8).

Discussion

Pilot study of rPOXA 1B stability

The pilot study demonstrated temperatures ranging between – 30 °C (243.15 K) and 40 °C (313.15 K), were appropriate to perform stability studies since at 40 °C (313.15 K) residual activity was of 61.30% (Table 1). In previous studies [40], rPOXA 1B demonstrated stability between 10 °C (283.15 K) and 50 °C (323.15 K); the temperature at which relative enzyme activity started to decrease. However, in that study, the exposure lasted only one hour. The pilot study demonstrated the negative effect of exposure time to elevated temperatures. The highest activity loss occurred at 50 °C during the first 15 days, with only 25.9% of the residual enzyme activity recovered, and then at 30 days, it further decreased to 13.2% relative enzyme activity (Table 1).

Prolonged exposure to elevated temperatures induces conformational changes that affect enzyme 3D structure [66]. Nevertheless, this is not common; it is more frequent during short time exposures. Li et al., (2017) evaluated thermal stability at 35 and 55 °C using commercial laccase (Lac), (Sigma, China). In this study, the authors found a relative enzyme activity loss of about 20% when the enzyme exposed for nine hours at 35 °C. Activity loss was about 60 and 100%, when the enzyme exposed during 1 and 9 h, respectively, at 55 °C, (323.15 K) [67]. The authors did not specify the origin of the enzyme, which is a crucial factor, because enzyme stability varies depending on origin and structure.

The sampling design proposed in this work allowed us to construct of a source population from which samples were randomly taken in each of the months (sampling moments). Henceforth in each case, the mean value of enzyme activity was always estimated with the same reliability and precision. The stratified sampling strategy made it possible to control data variations introduced because of using different batches, reducing the sampling error when estimating the enzyme activity mean values.

Analysis of real-time stability of rPOXA 1B concentrate

Proteins are generally more stable at freezing or refrigeration temperatures [24]. Nonetheless, stability depends on the enzyme's unaltered structure, hence its biological

function. Therefore, non-covalent interactions, such as Van del Waals, hydrophobic-, electrostatic-, and hydrogen-bonds are important [68, 69].

In this work at $-32.55 \pm 4.12\,°C$ $(240.98 \pm 5.38\,K)$, we observed that relative enzyme activity was high during the 12 months of the study (101.16%), (Fig. 1, Table 3). Eichlerová et al., (2015) described freezing laccase supernatant obtained from *Trametes versicolor* in liquid nitrogen $(-198\,°C, 75.15\,K)$, previous to $-80\,°C$ $(353.15\,K)$ storage, generated the highest enzyme activity loss in comparison to direct storage at $-80\,°C$ $(353.15\,K)$, [70]. Slow freezing processes produced ice crystals, whereas rapid freezing forms small and slender crystals in the protein's interfacial area, facilitating its denaturation [71].

Different investigations have analyzed the stability of laccase at freezing temperature, but very few (to the best of our knowledge) have evaluated exposure times longer than 12 months. Zhang et al., (2014) studied the residual activity of freeze-dried laccase from *T. versicolor* (Sigma-Aldrich) during 2 years of storage at $-20\,°C$ $(253.15\,K)$, finding a residual enzyme activity of 14.6% [72].

Refrigeration temperature is frequently to evaluate enzyme stability [31, 73]. At $4.32 \pm 1.22\,°C$ $(277.40 \pm 1.32\,K)$ rPOXA1B displayed a relative residual enzyme activity of 115.81% and a residual specific activity of $1045.58 \pm 15.31\,Umg^{-1}$; which implies it was stable during the 12 months of the study (Fig. 1). An increase in relative residual enzyme activity is infrequent, yet, Has-Schön et al., (2005) studied peroxidase (E.C. 1.11.1.) stability of a crude *Picea abies* extract at $4\,°C$ $(277.15\,K)$ for 30 days and found a relative residual enzyme activity of $\sim 190\%$. These variations are attributable to possible changes in the enzyme's native environment or the presence of substances that could have acted as activators [74].

In contrast Zhang et al., (2020) obtained a residual enzyme activity of only $10 \pm 1.1\%$ after 30-day storage at $4\,°C$ $(277.15\,K)$, using *Trametes versicolor* commercial laccase (Sigma-Aldrich), [31]. Bagewadi et al., (2017) monitored *Trichoderma harzianum* HZN10 laccase fining a 45% enzyme activity loss in only 8 days of storage at $4\,°C$ $(277.15\,K)$, [75]. Bou-Mitri and Kermasha, (2018) evaluated *Coriolus hirsutus* laccase, finding that after 4 weeks of storage at $4\,°C$ $(273.15\,K)$ the residual enzyme activity was 8.5% [73]. rPOXA1B relative residual stability results in this study demonstrated an enzyme with high stability, exceeding that of other laccases, which makes it a promising enzyme for high scale use.

In the present study at $24.99 \pm 0.25\,°C$ $(240.98 \pm 5.38\,K)$, $30.12 \pm 1.11\,°C$ $(303.27 \pm 1.11\,K)$ and $36.43 \pm 0.23\,°C$ $(309.58 \pm 0.23\,K)$ a reduced residual activity was observed with increasing temperature and exposure time, obtaining at the end of the study a relative enzyme activity from 76.43, 46.09 and 5.81%, respectively for each temperature (Fig. 1).

Enzyme denaturation at elevated temperatures is associated with an increase in the kinetic energy of the system, which generates conformational fluctuations despite between $25\,°C$ $(298.15\,K)$ and $100\,°C$ $(373.15\,K)$ the hydrophobicity appears to remain constant compared to other properties [32]. At $24.99 \pm 0.25\,°C$ $(297.53 \pm 3.88\,K)$ and $30.12 \pm 1.11\,°C$ $(303.27 \pm 1.11\,K)$ the residual enzyme activities were similar until the third month of exposure (Fig. 1), but in subsequent sampling. At $30.12 \pm 1.11\,°C$ $(303.27 \pm 1.11\,K)$ the enzyme activity decreased rapidly; an effect that could be due to irreversible thermal denaturation [76]. However, the stability of rPOXA 1B was higher than that reported for other laccases. Ahn et al., (2007) evaluated commercial laccase from *T. villosa* (Novo Nordisk - Danbury, CT), finding that storage for 30 days at $25\,°C$ $(298.15\,K)$ generated an exponential deactivation of the enzyme, with a loss of residual relative enzyme activity of 93% [77]. On the other hand, Nadar et al., (2019) evaluated commercial laccase from *T. versicolor* (Sigma-Aldrich), finding that after 18 days at $30\,°C$ $(303.15\,K)$ only 30% residual activity was obtained [78].

In the present study, we found that at $41.64 \pm 0.52\,°C$ $(314.79 \pm 0.52\,K)$ a considerable decrease in relative enzyme activity was observed, with a recovery of only 4.83% during the month of exposure, whereas in the pilot study relative residual enzyme activity at the same temperature was of 61.30% (Table 1, Fig. 2). In drug stability studies, lower concentrations generally support longer storage times [24]. This concentration effect also applies to biomolecules, since at high concentrations and temperatures enzymes are thermodynamically unstable and prone to form aggregates, due to hydrophobic groups exposure [79]. The difference between specific activity among concentrates used in the pilot study ($\sim 164.62\,Umg^{-1}$) and the stability study ($758.71 \pm 8.90\,Umg^{-1}$), demonstrates the number of enzyme units per milligram of protein was highest in the stability study. Tung et al., (2018) evaluated FIP-fve protein stability obtained from *Flammulina velutipes* at high and low concentrations during 1 min at $100\,°C$, recovering 16.4 and 85.0% of protein respectively. However, at $4\,°C$ $(277.15\,K)$ no changes were observed, recovering 100% of the protein regardless of the concentration used, yet at $-30\,°C$ $(303.15\,K)$ protein loss was slightly lower when the concentration was high [80].

rPOXA 1B accelerated stability and thermodynamics parameter analysis

The K_d for evaluated temperatures ranged between 3×10^{-3} and $0.400\,months^{-1}$, with a concomitant increase with the rise in temperature exposure (Table 4). This tendency has been previously observed due to enzyme and protein inactivation [78, 81]. K_d was used to

calculate the half-life ($t_{1/2}$), revealing that rPOXA 1B at − 32.55 ± 4.12 °C (240.98 ± 5.38 K) and 4.32 ± 1.22 °C (277.40 ± 1.32 K) was stable for at least for 230.7 and 46.2 months, respectively (Table 4).

The half-life ($t_{1/2}$) is an economically important factor since it allows to establish (according to conditions) expiration and storage dates for industrial or environmental applications, forasmuch as the higher the half-life ($t_{1/2}$) the higher the thermostability [82].

Certain reported $t_{1/2}$ values for other laccases have been lower. Yadav et al., (2018) evaluated recombinant small laccase rSLAC from *Streptomyces coelicolor* A3(2) produced in *P. pastoris* and obtained a $t_{1/2}$ of 60, 32 and 10 h at 60 °C (333.15 K), 70 °C (343.15 K) and 80 °C (353.15 K), respectively [83]. In contrast, using commercial *T. versicolor* (Sigma–Aldrich) laccase, Zhang et al., (2020) obtained a $t_{1/2}$ of 7.04, 5.63 and 5.38 h at 30 °C (303.15 K), 35 °C (308.15 K) and 45 °C (318.15 K), respectively [31].

E_d expresses thermal stability [78]. For rPOXA 1B an E_d of 41 KJ mol^{-1} was obtained (Fig. 3, Table 4), a value that is within the deactivation energy ranges reported by other authors. Nadar and Rathod, (2019) obtained 38.25 kJ mol^{-1} using commercial *T. versicolor* (Sigma–Aldrich) laccase, Maurya et al., (2020) attained 34.97 kJ mol^{-1} also using commercial *T. versicolor* laccase (Sigma–Aldrich), [84] and Ahn et al., (2007) obtained 25 kJ mol^{-1} using *Trametes villosa* laccase (Novo Nordisk - Danbury, CT), [77].

To the best of our knowledge POXA1B from *P. ostreutus* E_d has not been reported. However, the results herein obtained (E_d = 41 KJ mol^{-1}) confirm high stability for rPOXA 1B, because the highest energy is required to overcome the enzyme's inactivation barrier. It is known, changes in protein folding generate less organized and unstable molecules, due to the disruption of relatively weaker non-covalent bonds [85].

E_d is directly associated with enthalpy (ΔH), a thermodynamic parameter that expresses the total energy associated to enzyme denaturation. Large and positive E_d and ΔH values represent the high thermostability of the enzyme [86]. Positive ΔH values indicate that thermal deactivation is an endothermic reaction [76, 87], where the higher the ΔH value is, the highest the energy required to break the stabilizing bonds in a thermal inactivation of the enzyme [83]. Similar tendencies have reported for laccases and other enzymes [23, 76, 83]. Negative entropy values (ΔS) (Table 4) indicate the system has high stability, highest compactness and higher resistance to the thermal inactivation process [45], therefore a reasonable thermostability inside the temperature range studied. Thermal enzyme denaturation also results in the opening of the enzyme structure, accompanied by

an increase in the degree of disorder and randomness of the enzyme [86].

A very low or negative ΔG indicate spontaneous reactions and low stability [87]; a positive ΔG indicates resistance to denaturation, i.s. increased thermostability [88]. According to Agbo et al. (2017) an increase in ΔG when temperature raises, means high temperatures thermal stability [76]. However, such a tendency is rather uncommon. For *S. coelicolor* rSLAC laccase, a positive ΔG obtained without exhibit that trend [83]. Similar results were obtained by Filatova et al., (2019) using staphylolytic enzymes (Ply187AN-KSH3b and 2638aR), [23], which demonstrates data here obtained is in line with other investigations. ΔG is considered a more reliable stability indicator than ΔH and ΔS because it includes both enthalpic and entropic contributions [87, 88].

Effect of exposure to different temperatures on apparent V_{max} and K_M

Table 5 shows that V_{max} estimated from samples previously preserved between 240.98 K (− 32.55 °C) and 303.27 K (30.12 °C) is constant, suggesting the enzyme's reaction time was not affected, although at 303.27 K (30.12 °C) amplitude in the standard deviation was observed. At 309.58 K (36.43 °C) and 314.79 K (41.64 °C) the slight decrease in V_{max} could be explained by the effect of temperature on the enzyme. Michaelis-Menten (K_M) constant explains the affinity of an enzyme for a substrate, and the higher the K_M, the lower the affinity of the enzyme for the substrate, herein ABTS [84, 89]. In the present study average K_M and SD values progressively increased as temperature increased [240.98 K (− 32.55 °C) and 314.79 K (41.64 °C)]. The effect temperature has on K_M in other investigations has shown that K_M remains constant and without significant differences between 0 and 25 °C. Nonetheless, it presents a distinct threshold with an increase that can be significant at temperatures above 30 °C [90].

Homology modeling of POXA 1B

Sequence similarity is not the only factor determining 3D structure precision generated by homology. The minimum limit of sequence similarity in homology modelling should be 25% [91]; however, as a general rule, two sequences are homologous if they are more than 30% identical over their entire length. Notwithstanding, homologous sequences that share more than 40% identity are considered functionally similar [92]. In the three templates evaluated, the identity value was greater than 60%. QMEAN and GMQE scores were close to 1, suggesting the proposed model was of high quality and presented a high functional homology.

Based on the residue percentage in central regions in Ramachandran's plot, POXA 1B 3D structure had a high

stereochemical quality (Supplementary Material Figure 1). Verify score value suggested that 94.08% of the 3D modelled atoms were compatible with the sequence. Furthermore, the ERRAT score was adequate. Prognosticated protein models with a quality factor > 50% indicate the models by homology are stable and reliable [93], and the PROVES score was accepted, as it did not exceed 5%.

Our group previously reported a POXA 1B model using as template 1GYC [42]. Nevertheless, it was decided to improve and fine-tune the model using the semiautomatic MCPB.py Amber18 tool for molecules with metallic ion parametrization, since metallic complexes can have various modes of coordination [94], which are important for molecular dynamics analysis.

Molecular dynamics simulations and principal components analysis

RMSD determines the difference between the main chains of a protein from its initial to its final structural conformation, through the analysis of the deviations produced during the simulation (the minor deviation suggests higher stability of the system), [95]. RMSD calculation demonstrated the stability of the system at different temperatures was maintained during the simulation. Even though the RMSD deviation was higher with increasing temperatures, it remained low, stabilizing at an average of 0.96, 1.06, 1.26 and 1.20 Å for 241 K (−32.15 °C), 278 K (4.85 °C), 298 (24.85 °C) K and 314 K (40.85 °C), respectively.

Flexibility changes in a protein due to residue fluctuation can destabilize the system [59], where high Cα fluctuations are due to structural changes or free movements in the protein's backbone [96]. With the MD results, an RMSF and PCA analysis were implemented, to elucidate the effects an increase in temperature would have on the enzyme.

RMSF and PCA analyses complemented each other since PCA represent the residues and identified regions, which are similar in the RMSF analysis. However, to identify the differences in fluctuations among temperatures, Δ RMSF was evaluated using fluctuations of 241 K (− 32.15 °C) as the base temperature. The negative peaks observed in Δ RMSF analysis for LYS^{309} and ALA^{363} remained constant during exposure to different temperatures, indicating the stiffness of the system for those residues. LYS^{309} is found on a surface hairpin far from the active site, in the inter-dominium (D2-D3) region. ALA^{363} is found in D3, where the stiffness can be associated with strong interactions, generated by surrounding residues [97]. In contrast to the stiff residues, it was observed residues and flexible regions increased as the temperature was raised (Figs. 4A, 5). Flexible regions specify atom movements of the protein structure, as well

as weak interaction sites or regions of the enzyme [98]. Therefore, an increase of the flexible regions demonstrates loss of interactions or bonds that maintain the structure stiff.

ASP^{266}, ASN^{297} and nearby regions progressively increased the fluctuation with an increase in temperature (Figs. 4A, 5), shifting from a region with low fluctuation to one with high fluctuation between 278 and 314 K. Both residues, (ASP^{266}, ASN^{297}) are characterized by being hydrophilic and the nearby regions are composed of hydrophilic residues and residues of intermediate polarity. Hydrophilic residues are more fluctuating than hydrophobic [99]. Moreover, during MD simulations it is usual to observe an increase in flexibility in the hydrophobic regions. Furthermore, ASP^{266} and ASN^{297} residues are located in regions without a defined secondary structure, such as loops or coils; corresponding to regions of the highest fluctuations in any protein [100, 101]; as was observed during the analyses.

The region between LEU^{159} and VAL^{162} residues (Fig. 4A, 5) showed fluctuations in the three Δ RMSF analysis (278–241, 298–241 and 314–241 K). However, the region with the highest fluctuations was LEU^{159} and THR^{160}, which exhibited a higher fluctuation at 278 and 314 K; demonstrating temperature can increase or decrease residue fluctuations. Residue 162, which is not always VAL, has been studied in computational models for *Aspergillus oryzae* (PM1 and 7D5), [4] and *Coriolopsis trogii* [102] laccases, finding this residue is of great importance because it delimits the substrate-binding pocket and is characterized by having a wide network of hydrophobic interactions near CuT1.

The enzyme kinetic stability depends on the delicate balance between the flexibility and rigidity of its active site. The greater the stiffness of the active site, the greater the kinetic stability is [103]. The residues conserved and coordinated with copper ions obtained very low RMSF values, so they were not reported in the PCA. However, the fluctuation of PRO^{393} adjacent residue to HIS^{394}-(CuT1) could have generated instability in the system (at 314 K, 40.85 °C). Weakening of copper coordination or subtle rearrangements in the coordination sphere of CuT1 leads to alterations in the interconnection of residues, which could destabilise the entire active site structure resulting in loss of enzymatic activity [104].

Results demonstrated that experimental data (real-time stability studies) was supported by computational (molecular dynamics) since the MD simulated temperatures had high fluctuation regions that could influence the stability of the system, caused by high-temperature exposure, such as 314 K (40.8 °C). In the same way, the application of this computational approach can be used in other enzymatic systems by applying the same described protocols.

Conclusions

The stratified sampling allows to established population (N) and sample (n) size. The samples at each point in time (months) were random. This approach always allowed us to estimate the median value of the enzyme activity (UL^{-1}) with the same confidence (95%) and precision (21.8 UL^{-1}). Besides, it allows controlling the variation within the results since sampling was carried out from different batches, decreasing sampling error. This statistical approximation done in this research could be considered in other enzymes stability studies. We demonstrated that when rPOXA 1B concentrate (impure and without preservatives agents) stored at $-32.55 \pm 4.12\,°C$ (240.98 $\pm$ 5.38 K), $4.32 \pm 1.22\,°C$ (277.40 $\pm$ 1.32 K) or $24.99 \pm 0.25\,°C$ (297.53 $\pm$ 3.88 K) is stable with $t_{1/2}$ of 230.8, 46.2 and 12.6 months, respectively, exceeding reported storage time for other laccases. rPOXA 1B kinetic and thermodynamic parameters based on E_d (41.40 KJ mol^{-1}) and low K_M and V_{max} variations between $-32.55 \pm 4.12\,°C$ (240.98 $\pm$ 5.38 K) and $24.99 \pm 0.25\,°C$ (297.53 $\pm$ 3.88 K); as well as ΔH, ΔG and ΔS values, indicates the enzyme concentrate stability at different temperatures; making it even more attractive for industrial and environmental application. For POXA 1B active centre parametrisation, four coppers coordinated with the HIS^{394}, HIS^{496}, CYS^{451}, HIS^{64}, HIS^{397}, HIS^{66}, HIS^{109}, HIS^{111}, HIS^{399}, HIS^{450}, HIS^{452} residues; like the residues reported that coordinates with copper for other laccases. In general, at temperatures between 278 (4.85 °C) and 314 K (40.85 °C) (observed in the MD, using the Δ RMSF), all fluctuating residues were located at undefined secondary structure regions, such as loops or coils. Likewise, the number of residues with high fluctuations increased with temperatures changing from three residues (LEU^{159}, ALA^{391} and ASP^{429}) at 278 K (4.85 °C) to six residues (THR^{160}, ASP^{266}, GLU^{293}, ALA^{334}, ASP^{341} and LEU^{459}) at 298 K (24.85 °C) and nine residues (ASP^{101}, THR^{160}, GLY^{265}, ASN^{297}, ALA^{334}, GLY^{370}, ALA^{391}, PRO^{393} and ASP^{433}) at 314 K (40.85 °C). Real-time stability analyses and MD confirmed that the increase in temperature starkly affects POXA 1B activity. Temperature increases the fluctuations in hairpin, coils or loops; regions that mainly contain hydrophilic or intermediate polarity amino acids (ASP^{266} and ASN^{297}), favouring the long-term exposure of amino acids or hydrophobic zones that maintain the rigidity of the structure, resulting in irreversible inactivation of POXA 1B. At 314 K (40.85 °C), the PRO^{393} residue next to HIS^{394} (3.91 Å distance) increased the fluctuation and could result in the active site instability through alteration of the HIS^{394}-CuT1 coordination. This study identified temperatures (under assay conditions) for optimal long-term storage of rPOXA 1B concentrate; allowing the construction of a model based on experimentally assayed temperatures and using the Arrhenius equation to predict the enzyme's half-life ($t_{1/2}$) at temperatures ranging between 240.98 K (-32.55) and 309.58 K (36.43 °C). Our results are crucial to the technology transfer related to rPOXA 1B concentrate production at an industrial scale. Also, our findings help companies to decide to commercialise rPOXA 1B based on its multiple applications. Finally, our research group will continue the studies, using the pure enzyme and the addition of non-toxic preservatives to prolong the $t_{1/2}$ further.

Supplementary Information

The online version contains supplementary material available at https://doi.org/10.1186/s12896-021-00698-3.

Additional file 1.

Availability of data and materials
The raw data supporting the conclusions of this article will be may available by the authors, without undue reservation.

Ethics approval and consent to participate
Not applicable.

Consent for publication
Not applicable.

Author details
¹Departamento de Microbiología. Facultad de Ciencias. Pontificia Universidad
Javeriana (PUJ). Bogotá, Laboratorio de Biotecnología Molecular, Grupo de
Biotecnología Ambiental e Industrial (GBAI), Bogotá, D.C, Colombia.
²Vicerrectoría Académica. Universidad Antonio Nariño, Programa de Maestría
y Doctorado en Educación Matemática, Bogotá, D.C, Colombia.
³Departamento de Microbiología. Facultad de Ciencias. Pontificia Universidad
Javeriana (PUJ), Laboratorio de Biotecnología Aplicada, Grupo de
Biotecnología Ambiental e Industrial (GBAI), Bogotá, D.C, Colombia.
⁴Departamento de Química, Universidad Nacional de Colombia, Bogotá, D.C,
Colombia. ⁵Departamento de Microbiología. Facultad de Ciencias. Pontificia
Universidad Javeriana (PUJ). Bogotá, Laboratorio de Microbiología Ambiental
y de Suelos, Grupo de Biotecnología Ambiental e Industrial (GBAI), Bogotá,
D.C, Colombia.

References

1. Rivera-Hoyos CM, Morales-Álvarez ED, Poutou-Piñales RA, Pedroza-Rodríguez AM, Rodríguez-Vázquez R, Delgado-Boada JM. Fungal laccases. Fung Biol Rev. 2013;27(3–4):67–82. https://doi.org/10.1016/j.fbr.2013.07.001.
2. Awasthi M, Jaiswal N, Singh S, Pandey VP, Dwivedi UN. Molecular docking and dynamics simulation analyses unraveling the differential enzymatic catalysis by plant and fungal laccases with respect to lignin biosynthesis and degradation. J Biomol Struct Dyn. 2015;33(9):1835–49. https://doi.org/10.1080/07391102.2014.975282.
3. Stanzione I, Pezzella C, Giardina P, Sannia G, Piscitelli A. Beyond natural laccases: extension of their potential applications by protein engineering. Appl Microbiol Biotechnol. 2020;104(3):915–24. https://doi.org/10.1007/s00253-019-10147-z.
4. de Salas F, Cañadas R, Santiago G, Virseda-Jerez A, Vind J, Gentili P, et al. Structural and biochemical insights into an engineered high-redox potential laccase overproduced in Aspergillus. Int J Biol Macromol. 2019;141:855–67. https://doi.org/10.1016/j.ijbiomac.2019.09.052.
5. Yang J, Li W, Ng TB, Deng X, Lin J, Ye X. Laccases: production, expression regulation, and applications in pharmaceutical biodegradation. Front Microbiol. 2017;8:832.
6. Sharma A, Jain KK, Jain A, Kidwai M, Kuhad RC. Bifunctional in vivo role of laccase exploited in multiple biotechnological applications. Appl Microbiol Biotechnol. 2018;102(24):10327–43. https://doi.org/10.1007/s00253-018-9404-8.
7. Agrawal K, Chaturvedi V, Verma P. Fungal laccase discovered but yet undiscovered. Biores Biopro. 2018;5(1):4. https://doi.org/10.1186/s40643-018-0190-z.
8. Lettera V, Pezzella C, Cicatiello P, Piscitelli A, Giacobelli VG, Galano E, et al. Efficient immobilization of a fungal laccase and its exploitation in fruit juice clarification. Food Chemi. 2016;196:1272–8. https://doi.org/10.1016/j.foodchem.2015.10.074.
9. Castrovilli MC, Bolognesi P, Chiarinelli J, Avaldi L, Calandra P, Antonacci A, et al. The convergence of forefront technologies in the design of laccasebased biosensors e An update. Trends Anal Chem. 2019;119:115615. https://doi.org/10.1016/j.trac.2019.07.026.
10. Rojas-Higuera NS, Pava-Sánchez AM, Pinzón Rangel DL, Díaz-Ariza LA, Quevedo-Hidalgo B, Pedroza-Rodríguez AM. Bio-transformed sawdust by white rot fungi used as a carrier for plant growth-promoting bacteria. Eur J Wood Prod. 2017;75(2):263–73. https://doi.org/10.1007/s00107-016-1099-x.
11. Aghaie-Khouzani M, Forootanfar H, Moshfegh M, Khoshayand MR, Faramarzi MA. Decolorization of some synthetic dyes using optimized culture broth of laccase producing ascomycete Paraconiothyrium variabile. Biochem Eng J. 2012;60:9–15. https://doi.org/10.1016/j.bej.2011.09.002.
12. Morales-Álvarez ED, Rivera-Hoyos CM, Chaparro-Núñez LE, Daza CE, Poutou-Piñales RA, Pedroza-Rodríguez AM. Decolorization and detoxification of malachite green by Ganoderma lucidum: key operating parameters and adsorption studies. J Environ Eng. 2017;143(4):04016093. https://doi.org/10.1061/(ASCE)EE.1943-7870.0001180.
13. Ardila-Leal LD, Hernández-Rojas V, Céspedes-Bernal DN, Mateus-Maldonado JF, Rivera-Hoyos CM, Pedroza-Camacho LD, et al. Tertiary treatment (Chlorella sp.) of a mixed effluent from two secondary treatments (immobilized recombinant P. pastori and rPOXA 1B concentrate) of coloured laboratory wastewater (CLWW). 3 Biotech. 2020;10(5):233.
14. Rivera-Hoyos CM, Morales-Álvarez ED, Abelló-Esparza J, Buitrago-Pérez DF, Martínez-Aldana N, Salcedo-Reyes JC, et al. Detoxification of pulping black liquor with Pleurotus ostreatus or recombinant Pichia pastoris followed by CuO/TiO2/visible photocatalysis. Sci Rep. 2018;8(1):3503. https://doi.org/10.1038/s41598-018-21597-2.
15. Moreno-Bayona DA, Gómez-Méndez LD, Blanco-Vargas A, Castillo-Toro A, Herrera-Carlosama L, Poutou-Piñales RA, et al. Simultaneous bioconversion of lignocellulosic residues and oxodegradable polyethylene by Pleurotus ostreatus for biochar production, enriched with phosphate solubilizing bacteria for agricultural use. PLoS One. 2019;14(5):e0217100. https://doi.org/10.1371/journal.pone.0217100.
16. Gómez-Méndez LD, Moreno-Bayona DA, Poutou-Piñales RA, Salcedo-Reyes JC, Pedroza-Rodríguez AM, Vargas A, et al. Biodeterioration of plasma pretreated LDPE sheets by Pleurotus ostreatus. PLoS One. 2018;13(9): e0203786. https://doi.org/10.1371/journal.pone.0203786.
17. Margot J, Maillard J, Rossi L, Barry DA, Holliger C. Influence of treatment conditions on the oxidation of micropollutants by Trametes versicolor laccase. New Biotechnol. 2013;30(6):803–13. https://doi.org/10.1016/j.nbt.2013.06.004.
18. Maestre-Reyna M, Liu W-C, Jeng W-Y, Lee C-C, Hsu C-A, Wen T-N, et al. Structural and functional roles of glycosylation in fungal laccase from Lentinus sp. PLoS One. 2015;10(4):e0120601. https://doi.org/10.1371/journal.pone.0120601.
19. Pardo I, Camarero S. Laccase engineering by rational and evolutionary design. CMLS. 2015;72(5):897–910. https://doi.org/10.1007/s00018-014-1824-8.
20. Maté D, García-Burgos C, García-Ruiz E, Ballesteros AO, Camarero S, Alcalde M. Laboratory evolution of high-redox potential laccases. Chem Biol. 2010; 17(9):1030–41. https://doi.org/10.1016/j.chembiol.2010.07.010.
21. Senthivelan T, Kanagaraj J, Panda RC. Recent trends in fungal laccase for various industrial applications: An eco-friendly approach - a review. Biotechnol Bioprocess Eng. 2016;21(1):19–38. https://doi.org/10.1007/s12257-015-0278-7.
22. Mostafa FA. Abd El Aty AA: thermodynamics enhancement of Alternaria tenuissima KM651985 laccase by covalent coupling to polysaccharides and its applications. Int J Biol Macromol. 2018;120(Pt A):222–9. https://doi.org/10.1016/j.ijbiomac.2018.08.081.
23. Filatova L, Donovan D, Swift S, Pugachev V, Emelianov G, Chubar T, et al. Kinetics of inactivation of staphylolytic enzymes: qualitative and quantitative description. Biochim. 2019;162:77–87. https://doi.org/10.1016/j.biochi.2019.04.005.
24. Huynh-Ba K. Handbook of stability testing in pharmaceutical development. Springer Science+Business Media: Newark, Delaware; 2009. https://doi.org/10.1007/978-0-387-85627-8.
25. Christensen NJ, Kepp KP. Stability mechanisms of a thermophilic laccase probed by molecular dynamics. PLoS One. 2013;8(4):e61985. https://doi.org/10.1371/journal.pone.0061985.
26. Poonkuzhali K, Palvannan T. Thermostabilization of laccase by polysaccharide additives: enhancement using central composite design of RSM. Carb Polym. 2011;86(2):860–4. https://doi.org/10.1016/j.carbpol.2011.05.028.
27. Elias M, Wieczorek G, Rosenne S, Tawfik DS. The universality of enzymatic rate–temperature dependency. Trends Biochem Sci. 2014;39(1):1–7. https://doi.org/10.1016/j.tibs.2013.11.001.
28. Chen Y-C, Smith T, Hicks RH, Doekhie A, Koumanov F, Wells SA, et al. Thermal stability, storage and release of proteins with tailored fit in silica. Sci Rep. 2017;7(1):46568. https://doi.org/10.1038/srep46568.
29. Sanfelice D, Temussi PA. Cold denaturation as a tool to measure protein stability. Biophys Chem. 2016;208:4–8.
30. Rauk AP, Guo K, Hu Y, Cahya S, Weiss WF IV. Arrhenius Time-Scaled Least Squares: A Simple, Robust Approach to Accelerated Stability Data Analysis for Bioproducts. J Pharm Sci. 2014;103(8):2278–86. https://doi.org/10.1002/jps.24063.
31. Zhang R, Wang L, Han J, Wu J, Li C, Ni L, et al. Improving laccase activity and stability by HKUST-1 with cofactor via onepot encapsulation and its application for degradation of bisphenol a. J Hazard Mat. 2020;383:121130. https://doi.org/10.1016/j.jhazmat.2019.121130.
32. Pucci F, Rooman M. Physical and molecular bases of protein thermal stability and cold adaptation. Curr Opin Struct Biol. 2017;42:117–28. https://doi.org/10.1016/j.sbi.2016.12.007.

33. Papaleo E, Riccardi L, Villa C, Fantucci P, De Gioia L. Flexibility and enzymatic cold-adaptation: a comparative molecular dynamics investigation of the elastase family. Biochim Biophys Acta. 2006;1764:1397–406.

34. Quezada AG, DÍaz-Salazar AJ, Cabrera N, Pérez-Montfort R, Piñeiro Á, Costas M. Interplay between protein thermal flexibility and kinetic stability. Struct. 2017;25(1):167–79. https://doi.org/10.1016/j.str.2016.11.018.

35. Pikkemaat MG, Linssen ABM, Berendsen HJC, Janssen DB. Molecular dynamics simulations as a tool for improving protein stability. Protein Eng. 2002;15(3):185–92. https://doi.org/10.1093/protein/15.3.185.

36. Mohtashami M, Fooladi J, Haddad-Mashadrizeh A, Housaindokht MR, Monhemi H. Molecular mechanism of enzyme tolerance against organic solvents: insights from molecular dynamics simulation. Int J Biol Macromol. 2019;122:914–23. https://doi.org/10.1016/j.ijbiomac.2018.10.172.

37. Festa G, Autore F, Fraternali F, Giardina P, Sannia G. Development of new laccases by directed evolution: functional and computational analyses. Prot. 2008;72(1):25–34.

38. Monza E, Lucas MF, Camarero S, Alejaldre LC, Martínez AT, Guallar V. Insights into laccase engineering from molecular simulations: toward a binding-focused strategy. J Phys Chem Lett. 2015;6(8):1447–53. https://doi.org/10.1021/acs.jpclett.5b00225.

39. Hartmann J, Asch F. Extraction, storage duration, and storage temperature affect the activity of ascorbate peroxidase, glutathione reductase, and superoxide dismutase in Rice tissue. Biol. 2019;8:70.

40. Ardila-Leal LD, Albarracín-Pardo DA, Rivera-Hoyos CM, Morales ED, Poutou-Piñales RA, Cardozo-Bernal AM, et al. Media improvement for 10 L bioreactor production of rPOXA 1B laccase by *P. pastoris*. 3 Biotech. 2019; 9(12):447.

41. Pezzella C, Giacobelli VG, Lettera V, Olivieri G, Cicatiello P, Sannia G, et al. A step forward in laccase exploitation: recombinant production and evaluation of techno-economic feasibility of the process. J Biotechnol. 2017; 259:175–81. https://doi.org/10.1016/j.jbiotec.2017.07.022.

42. Rivera-Hoyos CM, Morales-Álvarez ED, Poveda-Cuevas SA, Reyes-Guzmán EA, Poutou-Piñales RA, Reyes-Montaño EA, et al. Computational analysis and low-scale constitutive expression of laccases synthetic genes *GILCC1* from *Ganoderma lucidum* and *POXA 1B* from *Pleurotus ostreatus* in *Pichia pastoris*. PLoS One. 2015;10(1):e0116524. https://doi.org/10.1371/journal.pone.0116524.

43. Lohr SL. Sampling, design and analysis, 2nd edition edn. USA: Chapman and Hall/CRC; 2019. https://doi.org/10.1201/9780429296284.

44. Melikoglu M, Ki Lin CS, Webb C. Kinetic studies on the multi-enzyme solution produced via solid state fermentation of waste bread by *Aspergillus awamori*. Biochem Eng J. 2013;80(15):76–82. https://doi.org/10.1016/j.bej.2013.09.016.

45. Gupta G, Sahai V, Gupta RK. Thermal stability and thermodynamics of xylanase from *Melanocarpus albomyces* in presence of polyols and salts. Bioresourcescom. 2014;9(4):5801–16.

46. Morales-Álvarez ED, Rivera-Hoyos CM, Cardozo-Bernal ÁM, Poutou-Piñales RA, Pedroza-Rodríguez AM, Díaz-Rincón DJ, et al. Plackett-Burman Design for rGILCC1 laccase activity enhancement in *Pichia pastoris*: Concentrated enzyme kinetic characterization. Enz Res. 2017;2017:5947581.

47. Nelson DL, Cox MM. Lehninger, principles of biochemistry. 7th ed. USA: W. H. Freeman and Company, Macmillan Higher Education; 2017.

48. Burquillo FJ, Holgado M, Bardsley WG. Uso del paquete estadístico SIMFIT en la enseñanza del análisis de datos en ciencias experimentales. J Sci Edu. 2003;4(1):8–14.

49. Zárate-Bonilla LJ, del Portillo P, Sáenz-Suárez H, Janneth G-S, Barreto-Sampaio GE, Poutou-Piñales RA, et al. Computational modeling and preliminary *iroN, fepA, cirA* gene expression in *Salmonella* Enteritidis under iron deficiency induced conditions. Poult Sci. 2014;93(1):221–30. https://doi.org/10.3382/ps.2012-02993.

50. Sáenz-Suárez H, Chávez-Zobbel A, Lareo LR, Oribio-Quinto C, Martínez-Mendoza J. Predicción computacional de estructura terciaria de las proteínas humanas Hsp27, aB-cristalina y HspB8. Univ Sci. 2011;16(1):15–28. https://doi.org/10.11144/javeriana.SC16-1.cpot.

51. Sáenz H, Lareo L, Poutou RA, Sosa C, Barrera LA. Predicción computacional de la estructura terciaria de la iduronato 2-sulfato sulfatasa humana. Bioméd. 2007;27(1):7–20. https://doi.org/10.7705/biomedica.v27i1.229.

52. Benkert P, Schwede T, Tosatto SC. QMEANclust: estimation of protein model quality by combining a composite scoring function with structural density information. BMC Struc Biol. 2009;9(1):35. https://doi.org/10.1186/1472-6807-9-35.

53. Benkert P, Tosatto SCE, Schomburg D. QMEAN: a comprehensive scoring function for model quality assessment. Prot. 2008;71(1):261–77.

54. Li P, Merz KM. MCPB.Py: a Python based metal center parameter builder. J Chem Inf Model. 2016;56(4):599–604. https://doi.org/10.1021/acs.jcim.5b00674.

55. Case DA, Belfon K, Ben-Shalom I, Brozell SR, Cerutti D, Cheatham T, et al. AMBER 2020. San Francisco: University of California; 2020.

56. Frisch MJ, Trucks GW, Schlegel HB, Scuseria GE, Robb MA, Cheeseman JR, Scalmani G, Barone V, Petersson GA, Nakatsuji H, Li X, Caricato M, Marenich AV, Bloino J, Janesko BG, Gomperts R, Mennucci B, Hratchian HP, Ortiz JV, Izmaylov AF, Sonnenberg JL, Williams-Young D, Ding F, Lipparini F, Egidi F, Goings J, Peng B, Petrone A, Henderson T, Ranasinghe D, Zakrzewski VG, Gao J, Rega N, Zheng G, Liang W, Hada M, Ehara M, Toyota K, Fukuda R, Hasegawa J, Ishida M, Nakajima T, Honda Y, Kitao O, Nakai H, Vreven T, Throssell K, Montgomery JA Jr, Peralta JE, Ogliaro F, Bearpark MJ, Heyd JJ, Brothers EN, Kudin KN, Staroverov VN, Keith TA, Kobayashi R, Normand J, Raghavachari K, Rendell AP, Burant JC, Iyengar SS, Tomasi J, Cossi M, Millam JM, Klene M, Adamo C, Cammi R, Ochterski JW, Martin RL, Morokuma K, Farkas O, Foresman JB, Fox DJ. Gaussian 16, revision A.03. Wallingford: Gaussian Inc.; 2016.

57. Maier JA, Martinez C, Kasavajhala K, Wickstrom L, Hauser K. Simmerling C: ff14SB: improving the accuracy of protein side chain and backbone parameters from ff99SB. J Chem Theory Comput. 2015;11(8):3696–713. https://doi.org/10.1021/acs.jctc.5b00255.

58. Roe DR, Cheatham TE III. PTRAJ and CPPTRAJ: software for processing and analysis of molecular dynamics trajectory data. J Chem Theory Comput. 2013;9(7):3084–95. https://doi.org/10.1021/ct400341p.

59. Acosta-Tapia N, Galindo JF, Baldiris R. Insights into the effect of Lowe syndrome-causing mutation p.Asn591Lys of OCRL-1 through protein –protein interaction networks and molecular dynamics simulations. J Chem Inf Model. 2020;60(2):1019–27. https://doi.org/10.1021/acs.jcim.9b01077.

60. Galindo-Murillo R, Roe DR, Cheatham TE III. On the absence of intrahelical DNA dynamics on the ms to ms timescale. Nat Commun. 2014;5(1):5152. https://doi.org/10.1038/ncomms6152.

61. Grant BJ, Rodrigues APC, ElSawy KM, McCammon JA, Leo S, Caves D. Bio3d: An R Package for the comparative analysis of protein structures. Bioinformatics. 2006;22(21):2695–6.

62. Peitsch M. ProMod and Swiss-model: internet-based tools for automated comparative protein modeling. Biochem Soc Trans. 1996;24(1):274–9. https://doi.org/10.1042/bst0240274.

63. Guez N, Peitisch MC. SWISS-MODEL and the Swiss-PdbViewer: An environment for comparative protein modeling. Electroph. 1997;18:2714–23.

64. Camacho C, Coulouris G, Avagyan V, Ma N, Papadopoulos J, Bealer K, et al. BLAST+: architecture and applications. BMC Bioinf. 2009;10(1):421. https://doi.org/10.1186/1471-2105-10-421.

65. Remmert M, Biegert A, Hauser A, Söding J. HHblits: lightning-fast iterative protein sequence searching by HMMhmm-alignment. Nat Met. 2011;9(2):173–5.

66. Lahmar I, Radeva G, Marinkova D, Velitchkova M. Belghith H, abdallah FB, Yotova L, Belghith K: immobilization and topochemical mechanism of a new β-amylase extracted from *Pergularia tomentosa*. Process Biochem. 2018; 64:143–51. https://doi.org/10.1016/j.procbio.2017.09.007.

67. Li G, Nandgaonkar AG, Wang Q, Zhang J, Krause WE, Wei Q, et al. Laccase-immobilized bacterial cellulose/TiO2 functionalized composite membranes: evaluation for photo- and bio-catalytic dye degradation. J Memb Sci. 2017; 525:89–98. https://doi.org/10.1016/j.memsci.2016.10.033.

68. Suplatov D, Panin N, Kirilin E, Shcherbakova T, Kudryavtsev P, Sˇvedas V. Computational design of a pH stable enzyme: understanding molecular mechanism of penicillin acylase's adaptation to alkaline conditions. PLoS One. 2014;9(6):e100643. https://doi.org/10.1371/journal.pone.0100643.

69. Kulshreshtha S, Chaudhary V, Goswami GK, Mathur N. Computational approaches for predicting mutant protein stability. J Comput Aided Mol Des. 2016;30(5):401–12. https://doi.org/10.1007/s10822-016-9914-3.

70. Eichlerova I, Homolka L, Tomsovsky M, Lisa L. Long term storage of *Pleurotus ostreatus* and *Trametes versicolo*r isolates using different cryopreservation techniques and its impact on laccase activity. Fungal Biol. 2015;119(12):1345–53. https://doi.org/10.1016/j.funbio.2015.10.004.

71. Roy I, Gupta MN. Freeze-drying of proteins: some emerging concerns. Biotechnol Appl Biochem. 2004;39(2):165–77. https://doi.org/10.1042/BA20030133.

72. Zhang X, Pan B, Wu B, Zhang W, Lu L. A new polymer-based laccase for decolorization of AO7: long-term storage and mediator reuse. Bioresour Technol. 2014;164:248–53. https://doi.org/10.1016/j.biortech.2014.04.105.

73. Bou-Mitri C, Kermasha S. Lyoprotection and stabilization of laccase extract from *Coriolus hirsutus*, using selected additives. AMB Exp. 2018;8(1):152. https://doi.org/10.1186/s13568-018-0683-3.

74. Has-Schön E, Lepeduš H, Jerabek L, Cesar V. Influence of storage temperature on total peroxidase activity in crude extracts from *Picea abies* L. Karst. Needles. Croatica Chem Acta. 2005;78(3):349–53.

75. Bagewadi ZK, Mulla SI, Ninnekar HZ. Purification and immobilization of laccase from *Trichoderma harzianum* strain HZN10 and its application in dye decolorization. J Genet Eng Biotechnol. 2017;15(1):139–50. https://doi.org/10.1016/j.jgeb.2017.01.007.

76. Agbo KU, Okwuenu PC, Ezugwu AL, Eze SOO, Chilaka FC. Thermostability and thermodynamic characterization of sprouted pearl millet alpha-amylases for its biotechnological applications. Bangladesh J Sci Ind Res. 2017;52(3):159–66. https://doi.org/10.3329/bjsir.v52i3.34146.

77. Ahn M-Y, Zimmerman AR, Martínez CE, Archibald DD, Bollag J-M, Dec J. Characteristics of *Trametes villosa* laccase adsorbed on aluminum hydroxide. Enz Microb Technol. 2007;41(1-2):141–8. https://doi.org/10.1016/j.enzmictec.2006.12.014.

78. Nadar SS, Rathod VK. Amino acid induced hyper activation of laccase and its application in dye degradation. Biocatal Agricult Biotechnol. 2019;18: 101064. https://doi.org/10.1016/j.bcab.2019.101064.

79. Vendruscolo M, Knowles TPJ, Dobson CM. Protein solubility and protein homeostasis: a generic view of protein misfolding disorders. Cold Spring Harb Perspect Biol. 2011;3(12):a010454.

80. Tung C-H, Lin C-C, Wang H-J, Chen S-F, Sheu F, Lu T-J. Application of thermal stability difference to remove flammutoxin in fungal immunomodulatory protein, FIP-fve, extract from *Flammulina velutipes*. J Food Drug Anal. 2018; 26(3):1005–14. https://doi.org/10.1016/j.jfda.2017.12.010.

81. Tavares APM, Silva CG, Drazic G, Silva AMT, Loureiro JM, Faria JL. Laccase immobilization over multi-walled carbon nanotubes: kinetic, thermodynamic and stability studies. J Colloid Interf Sci. 2015;454:52–60. https://doi.org/10.1016/j.jcis.2015.04.054.

82. Ahmed SA, Saleh SAA, Abdel-Hameed SAM, Fayad AM. Catalytic, kinetic and thermodynamic properties of free and immobilized caseinase on mica glass-ceramics. Heliyon. 2019;5(5):e01674. https://doi.org/10.1016/j.heliyon.2019.e01674.

83. Yadav D, Ranjan B, Mchunu N, Le Roes-Hill M, Kudanga T. Secretory expression of recombinant small laccase from *Streptomyces coelicolor* A3(2) in *Pichia pastoris*. Int J Biol Macromol. 2018;108:642–9. https://doi.org/10.1016/j.ijbiomac.2017.11.169.

84. Maurya SS, Nadar SS, Rathod VK. Dual activity of laccase-lysine hybrid organic–inorganic nanoflowers for dye decolourization. Environ Technol Innov. 2020;19:100798. https://doi.org/10.1016/j.eti.2020.100798.

85. Sant'Anna V, Cladera-Olivera F, Brandelli A. Kinetic and thermodynamic study of thermal inactivation of the antimicrobial peptide P34 in milk. Food Chem. 2012;130(1):84–9. https://doi.org/10.1016/j.foodchem.2011.07.001.

86. de Oliveira RL, da Silva OS, Converti A, Porto TS. Thermodynamic and kinetic studies on pectinase extracted from Aspergillus aculeatus: free and immobilized enzyme entrapped in alginate beads. Int J Biol Macromol. 2018;115:1088–93. https://doi.org/10.1016/j.ijbiomac.2018.04.154.

87. Miłek J. Thermodynamics and kinetics of thermal deactivation of catalase *Aspergillus niger*. Polish J Chem Technol. 2020;22(2):67–72.

88. Monteiro Souza PM, Aliakbarian B, Filho EX, Oliveira Magalhaes P, Junior AP, Converti A, et al. Kinetic and thermodynamic studies of a novel acid protease from Aspergillus foetidus. Int J Biol Macromol. 2015;81:17–21. https://doi.org/10.1016/j.ijbiomac.2015.07.043.

89. Kutcherlapati SNR, Yeole N, Jana T. Urease immobilized polymer hydrogel: long-term stability and enhancement of enzymatic activity. J Colloid Intef Sci. 2016;463:164–72. https://doi.org/10.1016/j.jcis.2015.10.051.

90. Razavi BS, Blagodatskaya E, Kuzyakov Y. Non linear temperature sensitivity of enzyme kinetics explains canceling effect—a case study on loamy haplic Luvisol. Front Microbiol. 2015;6:1126.

91. Muhammed MT, Aki-Yalcin E. Homology modeling in drug discovery: overview, current applications, and future perspectives. Chem Biol Drug Des. 2019;93(1):12–20. https://doi.org/10.1111/cbdd.13388.

92. Pearson WR. An Introduction to sequence similarity ("Homology") searching. Curr Prot Bioinformat. 2013;Chapter 3:Unit3.1.

93. Kameshwar AKS, Barber R, Qin W. Comparative modeling and molecular docking analysis of white, brown and soft rot fungal laccases using lignin model compounds for understanding the structural and functional

94. properties of laccases. J Mol Graph Model. 2018;79:15–26. https://doi.org/10.1016/j.jmgm.2017.10.019.

94. Merza JF, Cho MK. What are gene patents and why are people worried about them? Commun Genet. 2005;8(4):203–8.

95. Aier I, Varadwaj PK, Raj U. Structural insights into conformational stability of both wild-type and mutant EZH2 receptor. Sci Rep. 2016;6(1):34984. https://doi.org/10.1038/srep34984.

96. Singh SP, Gupta DK. A comparative study of structural and conformational properties of casein kinase-1 isoforms: insights from molecular dynamics and principal component analysis. J Theoret Biol. 2015;371:59–68. https://doi.org/10.1016/j.jtbi.2015.01.032.

97. Karshikoff A, Nilsson L, Ladenstein R. Rigidity versus flexibility: the dilemma of understanding protein thermal stability. FEBS J. 2015;282(20):3899–917. https://doi.org/10.1111/febs.13343.

98. Yu H, Huang H. Engineering proteins for thermostability through rigidifying flexible sites. Biotechnol Adv. 2014;32(2):308–15. https://doi.org/10.1016/j.biotechadv.2013.10.012.

99. Zhang T, Faraggi E, Zhou Y. Fluctuations of backbone torsion angles obtained from NMR-determined structures and their prediction. Prot. 2010; 78:3353–62.

100. Avelar M, Pastor N, Ramirez-Ramirez J, Ayala M. Replacement of oxidizable residues predicted by QM-MM simulation of a fungal laccase generates variants with higher operational stability. J Inorg Biochem. 2018;178:125–33. https://doi.org/10.1016/j.jinorgbio.2017.10.007.

101. Herrera-Zúñiga LD, Millán-Pacheco C, Viniegra-González G, Villegas E, Arregui L, Rojo-Domínguez A. Molecular dynamics on laccase from *Trametes versicolor* to examine thermal stability induced by salt bridges. Chemi Phys. 2019;517:253–64. https://doi.org/10.1016/j.chemphys.2018.10.019.

102. Mateljak I, Monza E, Lucas MF, Guallar V, Aleksejeva O, Ludwig R, et al. Increasing redox potential, redox mediator activity, and stability in a fungal laccase by computer-guided mutagenesis and directed evolution. ACS Catal. 2019;9(5):4561–72. https://doi.org/10.1021/acscatal.9b00531.

103. Xie Y, An J, Yang G, Wu G, Zhang Y, Cui L, et al. Enhanced enzyme kinetic stability by increasing rigidity within the active site. J Biol Chem. 2014; 289(11):7994–8006. https://doi.org/10.1074/jbc.M113.536045.

104. Durao P, Bento I, Fernandes AT, Melo EP, Lindley PF, Martins LO. Perturbations of the T1 copper site in the CotA laccase from *Bacillus subtilis*: structural, biochemical, enzymatic and stability studies. J Biol Inorg Chem. 2006;11(4):514–26. https://doi.org/10.1007/s00775-006-0102-0.

Publisher's Note

Springer Nature remains neutral with regard to jurisdictional claims in published maps and institutional affiliations.